Supplemental Information.
Title: Response to a pure tone in a nonlinear mechanical-electrical-acoustical model of the cochlea.
Julien Meaud and Karl Grosh.

1 Model parameters

The mechanical parameters and the OHC parameters of the cochlear model are listed in Tables S1 and S2. The values of the geometrical and electrical parameters can be found in [5] and [3].

Table S1: Mechanical parameters (x in cm).

Param.	Description	Value	Ref.
K_{bm}	BM stiffness per unit length	$2.1 \times 10^5 \exp(-3.5x) N/m^2$	[10]
D_{xx}	BM plate bending stiffness (xx)	$10^{-10} \exp(-0.5x) N.m$	[11]
D_{xy}	BM plate bending stiffness (xy)	$10^{-10} \exp(-0.5x) N.m$	[11]
D_{shear}	BM plate bending stiffness (shear)	$4.3 \times 10^{-11} \exp(-0.5x)$	[11]
K_{tms}	TM shear stiffness per unit length	$4.6 \times 10^4 \exp(-3.5x) N/m^2$	based on [12]
K_{tmb}	TM bending stiffness per unit length	$1.67 \times 10^4 \exp(-3.5x) N/m^2$	[13]
K_{rl}	RL stiffness per unit length	$1.4 \times 10^3 \exp(-2x) N/m^2$	fit
K_{ohc}	OHC stiffness per unit length	$1.4 \times 10^3 \exp(-2x) N/m^2$	fit
K_{st}	Stereocilia stiffness	$0.350 \exp(-3.6x) N/m$	[14]
M_{bm}	BM mass per unit length	$2.8 \times 10^{-7} kg/m$	based on [15]
M_{tms}	TM shear mass per unit length	$2.4 \times 10^{-6} \exp(0.5x) kg/m$	
M_{tmb}	TM bending mass per unit length	$1.2 \times 10^{-6} \exp(0.5x) kg/m$	
c_{bm}	BM damping coefficient per unit length	$0.085 Ns/m^2$	assumed
c_{hb}	HB damping coefficient	$\eta_f \frac{L_{tm}}{3L_{hb}}$, where η_f is the viscosity of the fluid, and L_{tm} and L_{hb} are the width and height of the subtectorial space	[3]
c_{tmb}	TM bending damping coefficient per unit length	$0.1 Ns/m^2$	assumed
G_{tms}	TM shear modulus	$7 \exp(-3.75x) kPa$	[16]
η_{tms}	TM shear viscosity	$0.03 Pa.s$	based on [4]

Table S2: OHC parameters (x in cm).

Parameter	Description	Value	Ref
G_m	basolateral conductance	$900 \exp(-3x) nS$	[7]
C_m	basolateral capacitance	9pF (base) to 21 pF (apex)	[7]
G_a^{max}	saturating HB conductance	$172 \exp(-2.05x) nS$	[6]
C_a	apical OHC capacitance	$0.5 pF$	see [5]
G_a^0	resting apical conductance	$P_0^s G_a^{max}$	
f_{gs}	single channel gating force	$10 pN$	[17]
ϵ_3	OHC electromechanical coupling coefficient	$-1.04 \times (10^{-5} + 10^{-6} x) N/m/mV$	[2]
P_0^s	resting probability	0.4	fit

2 Stapes displacement

The stapes displacement, u_{stapes}, is assumed to be given by:

$$u_{stapes}(\omega) = G(\omega) P_{stim} \tag{S1}$$

where P_{stim} is the pressure of the acoustic stimulation at the ear canal and $G(\omega)$ is a frequency dependent function. $G(\omega)$ is chosen as a quadratic function that fits the experimental data from Cooper [1] for the stapes vibrations of the guinea pig (see Fig. S1). The reference value is chosen so that 0dB relative to this reference value correspond to 0dB SPL in [9]. The results from simulations are then plotted as a function of the pressure P_{stim}, in dB SPL, so as to compare the model predictions with experimental data. The 2nd and 3rd harmonic components of the stapes displacement are assumed to be zero.

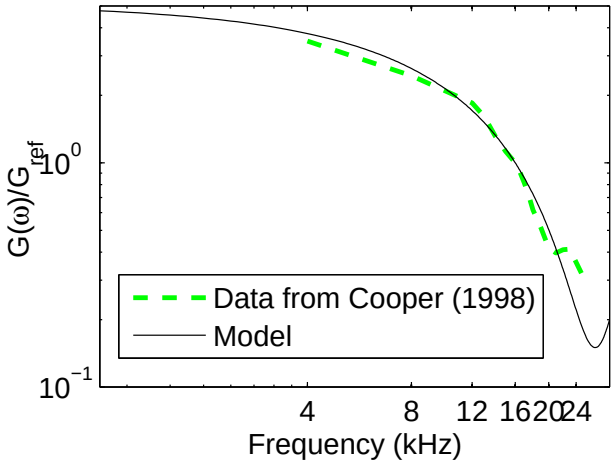

Figure S1: Stapes displacement. The data from Cooper [1] is fitted by a quadratic function $G(\omega)$ (see Eq. S1) to capture the frequency dependence of the stapes displacement.

3 Implementation of the alternative frequency time method

The governing equation governing the cochlear model in the frequency domain is given by Eq. 11. In the problem solved here, the only nonlinear term is in the structural electrical coupling (due to the nonlinearity of mechanoelectrical transduction), that depends only on the HB deflection, $u_{hb}(t)$ ($\mathbf{NL_m}\left[\mathbf{d}(t)\right] = \mathbf{NL_m}\left[\mathbf{u_{hb}}(t)\right]$). For a single tone stimulation, the right hand side, $(\mathbf{F_p})_\mathbf{m}$ is zero except for the fundamental ($m = 1$). The values of the variable $x(t)$ at the discrete time $t_q = \frac{(q-1)T}{N_{FFT}}$, where $q = 1,...,N_{FFT}$ and N_{FFT} is an integer, are denoted as x_q.

3.1 Algorithm: alternating frequency/time scheme

An iterative algorithm, named alternating frequency time (AFT) method and developed by Cameron and Griffin [8], is used to solve Eq. 11. The algorithm alternates between the frequency (to solve the system) and the time domains (to evaluate the nonlinear forcing term) using the Fourier and inverse Fourier transforms. For the problem considered here, the algorithm, based on a fixed point iteration, is the following:

1. Start with an initial guess ($k = 0$) in the frequency domain $\mathbf{D_m^{(0)}}$ where m=0,...,$N_h - 1$. We chose to start with $\mathbf{D_m^{(0)}} = \mathbf{0}$.

2. Start of iteration k. Calculate the HB deflection in the frequency domain $(\mathbf{U_{hb}})_{\mathbf{m}}^{(\mathbf{k})}$, where $m = 0,...,N_h - 1$, using the kinematic relation between the HB deflection and the BM and TM displacements.

3. Calculate the inverse fast Fourier transform (IFFT) of the HB deflection to obtain $(\mathbf{u_{hb}})_{\mathbf{q}}^{(\mathbf{k})}$, where $q = 1,...,N_{FFT}$.

4. Calculate the nonlinear forcing term, $\mathbf{nl}(\mathbf{d})$, at the discrete times t_q, $\mathbf{nl}(\mathbf{u_{hb}})_{\mathbf{q}}^{(\mathbf{k})}$, where $q = 1,...,N_{FFT}$, using Eq. 6.

5. Calculate the fast Fourier transform (FFT) of the nonlinear forcing term $\mathbf{nl}(\mathbf{u_{hb}})$ to obtain the nonlinearity in the frequency domain, $\mathbf{NL}(\mathbf{u_{hb}})_{\mathbf{m}}^{(\mathbf{k})}$

6. Solve the N_h linear systems given by Eq. 11. The nonlinear forcing term is set to $\mathbf{NL}(\mathbf{u_{hb}})_{\mathbf{m}}^{(\mathbf{k})}$. The solution of the system is denoted as $\mathbf{D}_{\mathbf{m}}^{(\mathbf{k+1})}$

7. Check for convergence. If converged, stop. If not, start the iteration $k + 1$.

For the DC shift, the algorithm described above does not converge. Therefore, a modified Newton's iteration is used instead of the fixed point iteration for the DC component. To limit the computational cost, the matrix $\frac{\partial \mathbf{NL}(\mathbf{u})}{\partial \mathbf{U}}$ is calculated only once, at the start of the first iteration. The other components of the response are computed with a fixed point iteration.

3.2 Implementation of the algorithm

At each iteration, the algorithm requires to solve one $n_{dof} \times n_{dof}$ linear system (where n_{dof} is the number of degrees of freedom) for each harmonic component. For each component, the matrix of the system depends only on the frequency. A LU decomposition algorithm is used to solve the linear systems. A typical simulation requires the computation of the solution for different intensity of stimulations (number of intensity of stimulation is defined as N_{input}) at different stimulus frequencies (the number of stimulus frequencies is defined as N_{freq}). To mimimize the computational cost, the computation is carried out in the following order:

1. For one stimulus frequency, calculate the matrices of the system for each harmonic component.

2. Compute the LU decomposition of the systems.

3. Compute the harmonic component of the solution for each magnitude of stapes displacement using the AFT algorithm and the LU decomposition previously computed.

4. Repeat the process for the next stimulus frequency.

3.3 Convergence and computational cost of the algorithm

The alternating time/frequency method introduces numerical error in the solution, due to three approximations: the finite number of discrete time points used for the FFT calculations, N_{FFT}, the finite number of harmonic components, N_h, and the finite number of iterations, N_{iter}. The value of N_{FFT} does not significantly affect the computational cost of the algorithm for the problem considered here (because the nonlinear forcing terms, $\mathbf{NL}(\mathbf{u})_{\mathbf{m}}^{(\mathbf{k})}$, depends only on a few degrees of freedom) and can be chosen sufficiently high (128 in the simulations) to obtain results with the desired accuracy.
The relative error in the BM displacement is plotted as a function of the number of iterations in Fig. S2, at CF and at CF/2. After 20 iterations the relative error in the fundamental is already less

than 0.1. However for the DC shift, 2nd and 3rd harmonic components, 30 iterations are required for the error to less than 0.1 at CF and about 0.1 at CF/2 (which is sufficient for our simulations).

The relative error is plotted as a function of N_h in Fig. S2 at CF and at CF/2. Obtaining the fundamental with a reasonable accuracy only requires the computation of the fundamental, as the relative error is about 0.01 both at CF and CF/2. The DC shift and the 2nd harmonic component requires the computation of three components (the DC shift, the fundamental and the 2nd harmonic). The 3nd harmonic requires the computation of four components.

This implementation of the algorithm requires the storage in memory of the LU decomposition of N_h matrices of size $n_{dof} \times n_{dof}$. The matrices are stored in memory using profile storage. The number of operations necessary to factorize each matrix is $c_1 = O(n_{dof} b^2)$ where b is the bandwidth of the matrix. The number of operations required to solve the system is $c_2 = O(n_{dof} b)$ for each iteration of the algorithm. The overall computation cost is:

$$c_{tot} = O\Big[\Big(n_{dof} b^2 + N_{iter} N_{input} n_{dof} b\Big) N_h N_{freq}\Big], \tag{S2}$$

where N_{iter} is the number of iterations required for convergence. The number of iterations and harmonic components required to obtain the converged components of the response of the BM, as well as the required memory and computational time are summarized in Table S3.

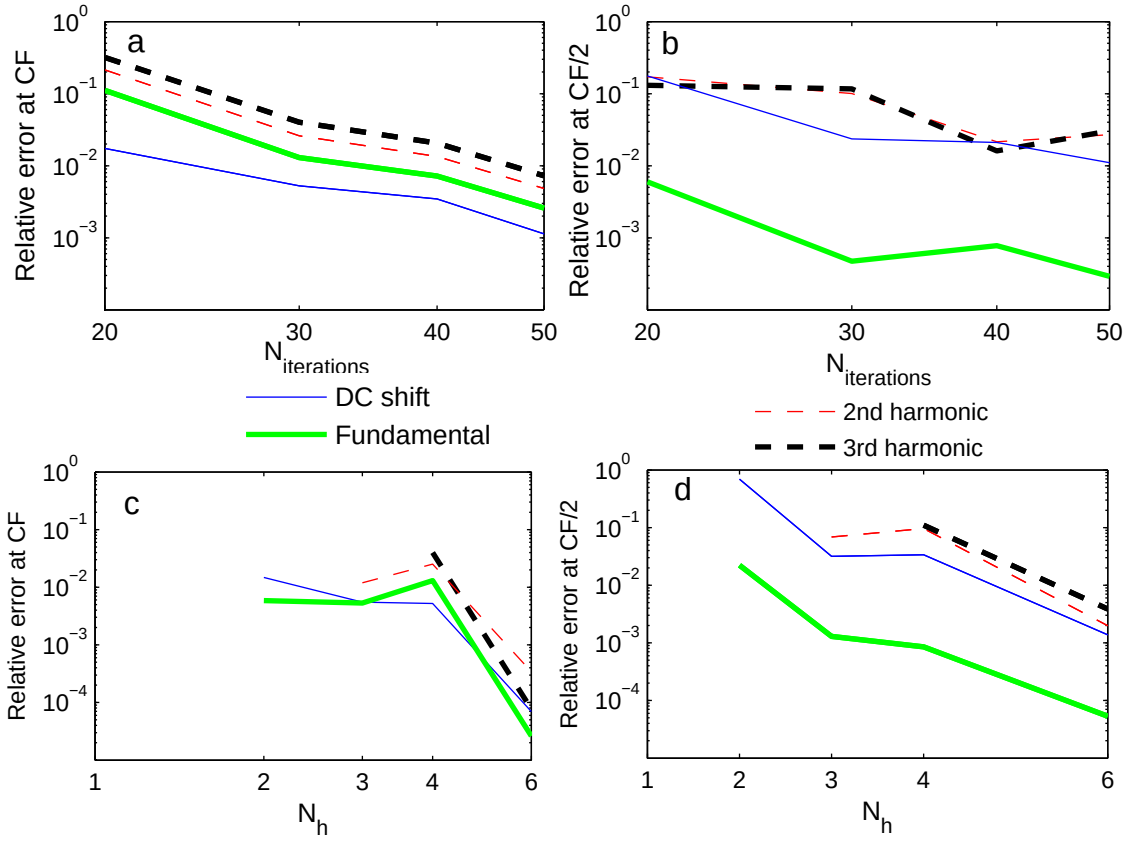

Figure S2: Convergence of the AFT algorithm. (a) and (b) Relative error in the BM displacement as a function of the number of iterations. The error is computed at CF (a) and at CF/2 (b) for the different harmonic components. The converged solution used as a reference for the computation of the relative error is the solution after 60 iterations. (c) and (d) Relative error in the BM displacement as a function of the number of harmonic components. The error is computed at CF (c) and at CF/2 (d). The converged solution used for reference for the computation of the relative error is the solution with 8 harmonic components. All simulations in (c) and (d) are with 30 iterations.

Table S3: Number of harmonic components, number of iterations, memory and computational time required for convergence.

Component	N_h	N_{iter}	Required RAM	Computational time $N_{freq} = 1$ $N_{input} = 1$	Computational time $N_{freq} = 200$ $N_{input} = 15$
Fundamental	1	< 20	1.40GB	13s	4.5 hours
DC	3	30	2.32GB	52s	22.0 hours
2nd harmonic	3	30	2.32GB	52s	22.0 hours
3rd harmonic	4	30	3.77GB	68s	28.2 hours
Linear	1	1	0.688GB	10s	8.4 hours

4 Response at different longitudinal locations

The response to single tone simulation at different locations is shown in Fig. S3. As the location moves from the basal to more apical locations, the peak of the fundamental BM response shifts to lower frequencies (Fig. S3(a)). The peak of the response at low intensity (4dB SPL) becomes lower and less sharp as the location approaches the apex. At the most apical locations, the response at low intensity is indistinguishable from the response at high intensity of stimulation.

As seen in Fig. S3(b), the magnitude of the TM bending mode relative to the fundamental decreases from basal locations (high CF) to more apical locations (low CF). For CF greater than about 5kHz, the TM bending mode is more sensitive than the BM. The TM shearing mode is more sensitive than the BM for CF greater than about 15kHz. The magnitude of the DC shift at 104dB SPL in the BM (respectively on the TM bending mode) increases from 0.6nm (respectively 6nm) for a CF of 25kHz to 6nm (respectively 23nm) for a CF of 6.5kHz. The DC shift for lower CF is lower, with a magnitude of about 0.9nm (respectively 2nm) for a CF of 2kHz. The variation of the DC shift with the CF can be explained to first order by the lower stiffness of the BM and TM bending mode towards the apex. The solid lines for the DC shift on the BM and on the TM bending mode corresponds to the following equations:

$$u_{bm}^{DC}(x) = \frac{\epsilon_3 \Delta\phi_{ohc}^{DC}}{K_{bm}(x)} \tag{S3}$$

$$u_{tmb}^{DC}(x) = \frac{\epsilon_3 \Delta\phi_{ohc}^{DC}}{K_{tmb}(x)} \tag{S4}$$

where ϵ_3 and the DC shift in the OHC transmembrane potential, $\Delta\phi_{ohc}^{DC}$, are assumed to be independent of x.

The 2nd harmonic is approximately within 30dB of the fundamental for stimulus frequency equal to CF, for CF between 25kHz and 6.5kHz (Fig. S3(d)); for lower CF, the 2nd harmonic is lower. For stimulus frequency equal to CF/2, the 2nd harmonic is approximately within 15dB of the fundamental for CF between 25 and 12kHz; at more apical locations, the 2nd harmonic is much lower. The fundamental and DC shift in the transmembrane potential are approximately independent of the CF for CF between 25 and 3kHz.

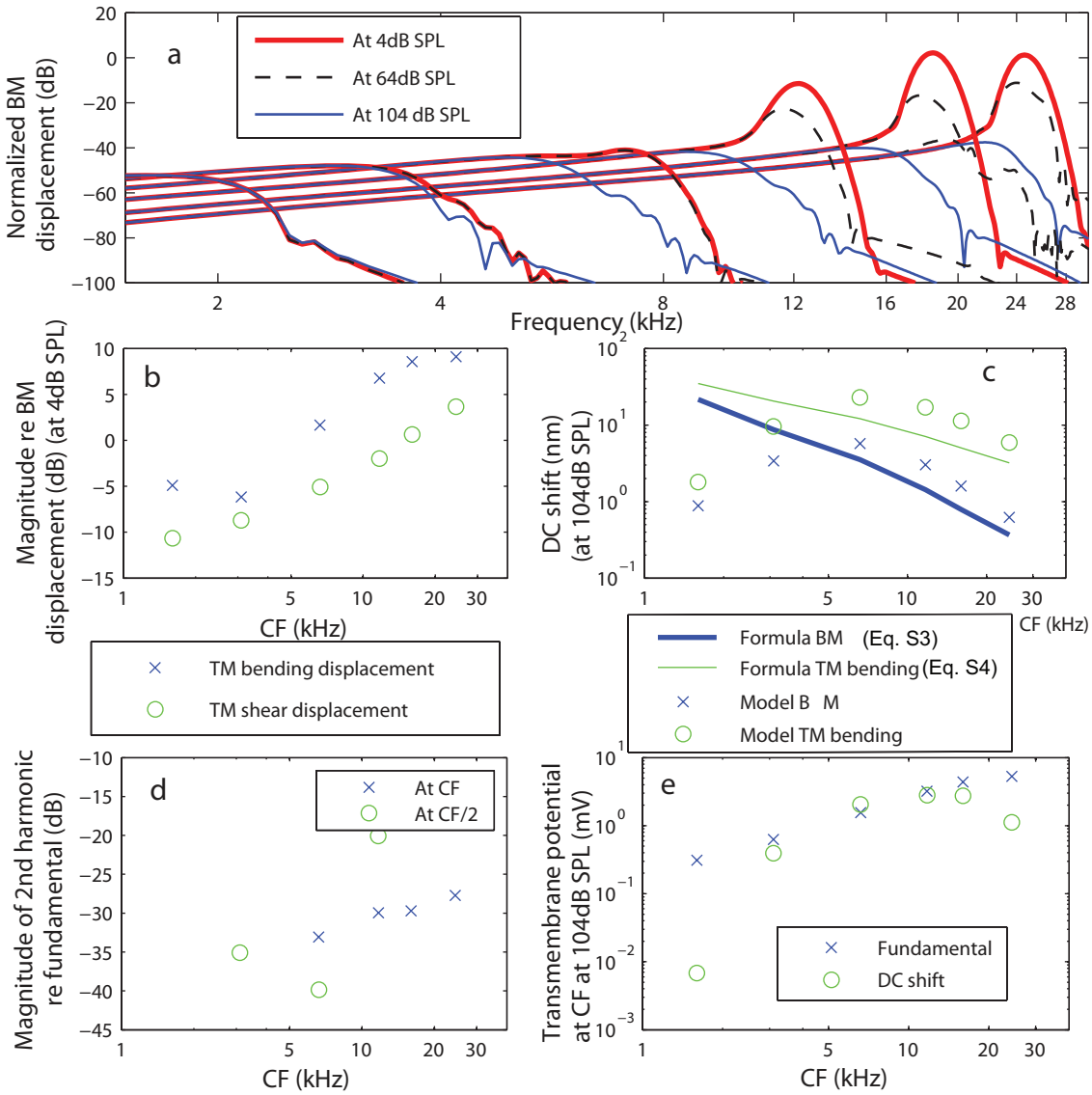

Figure S3: Response at different locations. a. Fundamental of the BM response as a function of frequency at locations 0.25cm, 0.46cm, 0.62cm, 0.87cm, 1.12cm and 1.37cm from the base of the cochlea. b. Magnitude of the TM shear and bending displacement relative to the stapes displacement as a function of the CF of the location. c. Magnitude of the DC shift in the BM and TM bending mode at CF at 104dB SPL as a function of the CF. d. Magnitude of the 2nd harmonic relative to the fundamental at CF (crosses) and at CF/2 (circles) as a function of the CF. e. Magnitude of the fundamental and DC shift in the OHC transmembrane potential at 104dB SPL as a function of the CF.

Supporting references

[1] Cooper, N. P. 1998. Harmonic distortion on the basilar membrane in the basal turn of the guinea-pig cochlea. *J. Phys. (Lond.)*, 509(1):277–288.

[2] Iwasa, K. H., and M. Adachi. 1997. Force generation in the outer hair cell of the cochlea. *Biophys. J.*, 73:546–555.

[3] Meaud,J. and K. Grosh. The effect of tectorial membrane and basilar membrane longitudinal coupling in cochlear mechanics. *J. Acoust. Soc. Am.*, 127(3):1411–1421, 2010.

[4] Ghaffari, R., Aranyosi, A. J., and D. M. Freeman. 2007. Longitudinally propagating traveling waves of the mammalian tectorial membrane. *Proc. Natl. Acad. Sci. USA*, 104(42):16510–16515.

[5] Ramamoorthy, S., Deo, N. V., and K. Grosh. 2007. A mechano-electro-acoustical model for the cochlea: Response to acoustic stimuli. *J. Acoust. Soc. Am.*, 121:2758–2773.

[6] He, D. Z. Z., Jia, S. P., and P. Dallos. 2004. Mechanoelectrical transduction of adult outer hair cells studied in a gerbil hemicochlea. *Nature*, 429(6993):766–770.

[7] Johnson, S.L., Beurg, M., Marcotti, W., and R. Fettiplace. 2011. Prestin-driven cochlear amplification is not limited by the outer hair cell membrane time constant. *Neuron*, 70:1143-1154.

[8] Cameron, T. M., and J. H. Griffin. 1989. An alternating frequency/time domain method for calculating the steady-state response of nonlinear dynamic systems. *J. Appl. Mech. T. ASME*, 56(1):149–154.

[9] J. F. Zheng, N. Deo, Y. Zou, K. Grosh, and A. L. Nuttall. Chlorpromazine alters cochlear mechanics and amplification: In vivo evidence for a role of stiffness modulation in the organ of corti. *J. Neurophysiol.*, 97(2):994–1004, 2007.

[10] Gummer, A. W., B. M. Johnstone, and N. J. Armstrong. 1981. Direct measurement of basilar membrane stiffness in guinea pig. *J. Acoust. Soc. Am.*, 70(5):1298–1309.

[11] Liu, S. and R. D. White. 2008. Orthotropic material properties of the gerbil basilar membrane. *J. Acoust. Soc. Am.*, 123(4):2160–2171.

[12] Richter, C. P., G. Emadi, G. Getnick, A. Quesnel, and P. Dallos. 2007. Tectorial membrane stiffness gradients. *Biophys. J.*, 93:2265–2276.

[13] Zwislocki, J. J. and L. K. Cefaratti. 1989 Tectorial membrane ii: Stiffness measurement in vivo. *Hear. Res.*, 42(2-3):211–228.

[14] Strelioff, D., A. Flock, and K.E. Minser. 1985. Role of inner and outer-hair-cells in mechanical frequency-selectivity of the cochlea. *Hear. Res.*, 18(2):169–175.

[15] C. Fernandez. 1952. Dimensions of the cochlea (guinea pig). *J. Acoust. Soc. Am.*, 24(5):519–523.

[16] Gavara, N. and R.S. Chadwick. 2009. Collagen-based mechanical anisotropy of the tectorial membrane: implications for inter-row coupling of outer hair cell bundles. *PLoSOne*, 4:e4877.

[17] Beurg, M., J. H. Nam, A. Crawford, and R. Fettiplace. 2008. The actions of calcium on hair bundle mechanics in mammalian cochlear hair cells. *Biophys. J.*, 94:2639–2653.